Applied Catalysis B: Environmental 128 (2012) 55–63

Contents lists available at SciVerse ScienceDirect

Applied Catalysis B: Environmental

journal homepage: www.elsevier.com/locate/apcatb

Study by electrical conductivity measurements of semiconductive and redox properties of ceria and phosphated ceria catalysts

Ionel Popescu, Ioan-Teodor Trotuş, Ioan-Cezar Marcu*

Laboratory of Chemical Technology & Catalysis, Department of Organic Chemistry, Biochemistry & Catalysis, Faculty of Chemistry, University of Bucharest, 4-12, Blv. Regina Elisabeta, 030018, Bucharest, Romania

ARTICLE INFO

Article history:
Available online 3 March 2012

Dedicated to Jean-Marie Herrmann, the scientist, the professor and the man.

Keywords:
Electrical conductivity
Ceria
Phosphated ceria
Catalytic oxydehydrogenation
Isobutane

ABSTRACT

Pure ceria and two surface-phosphated ceria containing different amounts of phosphorus, 1.1P/CeO_2 and 2.2P/CeO_2, catalysts for isobutane oxydehydrogenation, were characterized by in situ electrical conductivity measurements. Their electrical conductivity was studied as a function of temperature and oxygen partial pressure and was followed with time during sequential exposures to air, nitrogen, isobutane–air mixture (reaction mixture) and isobutane–nitrogen mixture in conditions similar to those of catalysis. All the materials appeared to be *n*-type semiconductors under air with quasi-free electrons as the main charge carriers and their electrical conductivity increased following the order: CeO_2 < 1.1P/CeO_2 < 2.2P/CeO_2. While CeO_2 and 1.1P/CeO_2 remained *n*-type semiconductors when contacted with isobutane–nitrogen or isobutane–air mixture, 2.2P/CeO_2 became a *p*-type semiconductor with positive holes as the main charge carriers. For 2.2P/CeO_2 catalyst the oxydehydrogenation reaction involves surface lattice O^- species, whereas for CeO_2 surface lattice O^{2-} anions are involved. For 1.1P/CeO_2 catalyst the reaction mechanism involves both surface lattice O^{2-} anions and surface lattice O^- species. These results explained the difference in catalytic performances encountered on these solids. In all cases the overall reaction mechanism can be assimilated to a Mars and van Krevelen mechanism.

1. Introduction

Electrical conductivity measurements carried out on oxides used as catalysts in oxidation reactions involving redox processes between reactants and catalysts can provide information on the nature of surface structure defects, the existence of oxidizing species (ionosorbed oxygen species, active surface anions) and the nature of the oxidic phase involved in catalytic reactions as described in Ref. [1]. The electrical behavior of these catalysts is generally a function of the temperature, whose influence can be followed in the same range as that of catalysis, of the oxygen pressure and of the nature of the gas phase in contact with the solid. Consequently, electrical conductivity measurements constitute a useful tool to characterize oxidation catalysts and the literature data show that it has largely been used [2–13], some of the most interesting results obtained being resumed below. Herrmann et al. [4] established the *p*-type character of the V-P-O catalysts used for the partial oxidation of *n*-butane to maleic anhydride and clearly evidenced the redox mechanism involved with the initial hydrogen abstraction from *n*-butane by O^- species from surface V^{4+}—O^- pairs. Using the same technique, a change in the nature of the semiconductivity that passes from *p*-type under air to *n*-type under *n*-butane–air reaction mixture was evidenced for Ti and Zr pyrophosphates used as catalysts for the oxydehydrogenation of *n*-butane, and a reaction mechanism involving surface O^- species was proposed [5,6]. The same reaction was studied over promoted and unpromoted nickel molybdates and by using the electrical conductivity measurements the *n*-type character of the solids and the role of the promoter have been established and a redox-type reaction mechanism has been proposed [7,8]. Millet et al. [10] studied by electrical conductivity measurements V-Sb-(Fe)-O catalysts which are active in the ammoxidation of propane, and found that an increased concentration of cationic vacancies and isolated V^{4+} species, due to the introduction of increasing amounts of Fe in the lattice, led to a proportionally higher activity. Barium and lead perovskites, catalysts for the total oxidation of methane, were also studied using this method [12]. For both perovskites, the alkane activation was proposed to be related to the *p*-type semiconducting properties of the solids, likely through hydrogen abstraction by a surface O^- species. Moreover, it has been shown that the higher the concentration of O^- species, the greater the catalytic activity. Supported oxide-based catalysts, such as V_2O_5-WO_3/TiO_2 used in selective catalytic reduction (SCR) deNO_x reaction, have also been studied by means of electric conductivity measurements [13]. It

* Corresponding author. Tel.: +40 214103178x138; fax: +40 213159249.
E-mail address: ioancezar.marcu@g.unibuc.ro (I.-C. Marcu).

0926-3373/$ – see front matter © 2012 Elsevier B.V. All rights reserved.
doi:10.1016/j.apcatb.2012.01.037

has been shown that the SCR deNO$_x$ reaction over V_2O_5-WO_3/TiO_2 catalyst is a redox process assisted by acidic sites necessary for the dissociative chemisorption of ammonia.

It is important to point out that there are several studies concerning the use of ceria and CeO_2-containing materials as catalysts or catalysts' supports, a book being already devoted to this topic [14]. Also, several studies concerning the electrical properties of pure and doped ceria have already been performed and reviewed in Refs. [14,15]. The electrical properties of these materials are mainly associated to the presence of oxygen vacancies also recognized to play a key role in the catalytic activity by improving the lattice oxygen mobility and lability, and, for the noble metals supported on ceria-based materials, by favoring the electronic transfer from the support to the noble metal [16].

In the present work DC-electrical conductivity of ceria and phosphated ceria was studied as a function of the temperature, the air pressure, the nature of different gaseous reactant atmospheres and the reaction mixture. Reaction mechanisms for the transformation of isobutane over these catalysts have been proposed and a correlation between their semiconductive and catalytic properties has been established.

2. Experimental

2.1. Catalysts preparation and characterization

The phosphated ceria samples were prepared by adding to the fine grounded ceria (Merck) a 1.1 M or 2.2 M $NH_4H_2PO_4$ solution adjusted to pH of 7 with NH_4OH, as described elsewhere [17]. After stirring for about 20 min, the solution was drained from the solid which was then dried at 100 °C and finally calcined in air for 2 h at 400 °C followed by 3 h at 700 °C. They were labeled 1.1P/CeO_2 and 2.2P/CeO_2, respectively.

The crystal structure of the compounds was controlled by X-ray diffraction. All the solids showed a well crystallized ceria phase having the fluorite structure and for the phosphated samples weak reflections corresponding to $CePO_4$ (monazite) phase were also observed [17]. The BET surface areas of the CeO_2, 1.1P/CeO_2 and 2.2P/CeO_2 samples were equal to 6.4, 3.3 and 2.6 $m^2\,g^{-1}$, respectively.

2.2. Catalytic test

The catalytic oxydehydrogenation of isobutane was performed in a fixed bed quartz tube down-flow reactor operating at atmospheric pressure, in the temperature range from 450 to 610 °C, as described elsewhere [17]. The gas feed consisted of an isobutane–air mixture (air/isobutane molar ratio equal to 2.5). The volume hourly space velocity (VHSV) with respect to isobutane was maintained at 1000 h^{-1}. The reaction products were analyzed by gas chromatography. The major products formed were isobutene, CO, CO_2 and cracking products (methane and propylene).

2.3. Electrical conductivity measurements

The samples were compressed at ca. 2.76×10^7 Pa using a Carver 4350.L pellet press to ensure good electrical contacts between the catalyst grains. The obtained pellet was then placed in a horizontal quartz tube between two platinum electrodes. Flow rates of gases flowing over the sample were controlled by fine needle valves and were measured by capillary flow meters. The temperature was controlled using thermocouples soldered to the electrodes and, when short-circuited, they were used to determine the electrical conductivity σ of the samples, which can be expressed by the formula:

$$\sigma = \frac{1}{R} \times \frac{t}{S} \quad (1)$$

where R is the electrical resistance and t/S is the geometrical factor of the pellet including the thickness t (ca. 3 mm) and the cross sectional area S of the pellet whose diameter was equal to 13 mm. The electrical resistance was measured with a megaohmmeter (FLUKE 177 Digital Multimeter).

To compare the electrical conductivities of the samples, it is required that the solids have similar textures and identical surface states. This requirement is easily fulfilled since all the samples have similar textures. Indeed, the electrical conductivity of semiconducting oxide powders can be written as:

$$\sigma = An \quad (2)$$

where n is the concentration of the main charge carriers and A is a coefficient of proportionality which includes the mobility of the main charge carriers and the elementary charge of the electron and depends on the compression of the powder and on the number and quality of contact points between particles [1]. Since the samples were compressed at the same pressure and have similar BET surface areas and since the electrical measurements were standardized, A can be considered as identical for all the samples under identical conditions.

The common reference state for σ determination has been chosen under air at atmospheric pressure and at 490 °C or 610 °C. At these temperatures, which are in the range used in the catalytic reactions, most of the ionically adsorbed species such as H_3O^+, HO^- which would produce an additional surface conductivity are eliminated. The solid was initially heated from room temperature to the desired temperature at a heating rate of 5 °C/min.

3. Results and discussion

3.1. Catalytic performances

Although the present work is devoted to the electrical and redox properties of ceria and phosphated ceria, it is important to mention about their catalytic performances in isobutane oxydehydrogenation. They are presented in Table 1 for the reaction at 490 and 610 °C. It can be observed that, at 490 °C, by adding phosphorus to ceria and by increasing its content, the catalytic activity decreased with an important increase of the selectivity for isobutene mainly at the expense of the combustion products, the less active but the most selective catalyst in this series being 2.2P/CeO_2 catalyst. This tendency was observed for temperatures up to 570 °C [17]. At higher temperatures, such as 610 °C, both the activity and the selectivity increased by adding phosphorus to ceria and by increasing its content. Thus, at higher temperatures, 2.2P/CeO_2 catalyst became the most active as well as the most selective one. This behavior corresponds to a compensation effect in catalysis, 570 °C being the isokinetic temperature. The catalytic performances resumed here were in detail discussed in Ref. [17].

3.2. Electrical conductivity measurements

3.2.1. Variations of the electrical conductivity as a function of temperature

The electrical conductivities of the ceria and phosphated ceria samples have been measured as a function of temperature to determine the activation energy of conduction E_c, under air at atmospheric pressure, in the temperature range from 400 to 660 °C. The semi-log plots [$\log\sigma = f(1/T)$] obtained are given in Fig. 1. The linear variations observed showed that all the compounds behaved

Table 1
Catalytic performances of ceria and phosphated ceria in the reaction of isobutane.[a]

Catalyst	Reaction temperature (°C)	Isobutane conversion (%)	Selectivities (%)		
			Isobutene	CO_x	Cracking
CeO_2	490	8.0	34.2	46.2	19.6
	610	11.8	26.1	26.8	47.1
1.1P/CeO_2	490	6.5	71.2	12.5	16.3
	610	13.5	49.2	5.2	45.6
2.2P/CeO_2	490	5.5	90.0	7.4	2.6
	610	14.7	68.4	5.1	26.5

[a] Reaction conditions: air/isobutane molar ratio = 2.5, VHSV with respect to isobutane = 1000 h^{-1}.

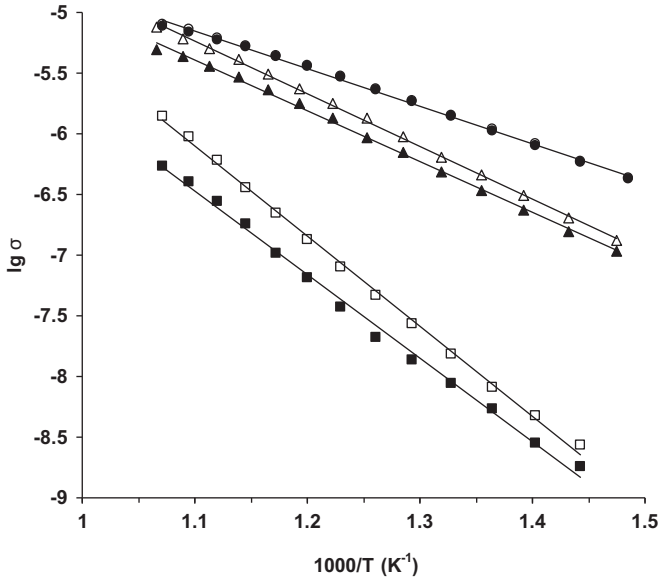

Fig. 1. Arrhenius plots for the electrical conductivity σ of CeO_2 (■, □), 1.1P/CeO_2 (▲, △) and 2.2P/CeO_2 (●, ○) under air (filled symbols) and under nitrogen (open symbols) (σ in Ω^{-1} cm^{-1}).

as semiconductors whose electrical conductivities varied exponentially with temperature according to the typical activation law:

$$\sigma = \sigma_0 \ \exp\left(-\frac{E_c}{RT}\right) \quad (3)$$

where σ_0 is the pre-exponential factor. The slopes of the semi-log plots enabled one to calculate the E_c values presented in Table 2. It can be observed that the activation energy of conduction decreased by adding phosphorus to ceria and by increasing its content. It is noteworthy that the electrical conductivity of the samples increased following the order: CeO_2 < 1.1P/CeO_2 < 2.2P/CeO_2. This means, according to Eq. (2), that the concentration of charge carriers increased by adding phosphorus to ceria and by increasing its content.

The electrical conductivities of the catalysts have also been measured as a function of temperature under nitrogen at atmospheric pressure (Fig. 1) for determining the nature of the semiconductor type of the solid by applying the Heckelsberg criterion [18].

Table 2
Electrical characteristics of ceria and phosphated ceria samples.

Catalyst	E_c (kJ mol^{-1})[a]	Exponent n[b]
CeO_2	139.8	4
1.1P/CeO_2	80.9	20
2.2P/CeO_2	59.6	–

[a] Activation energy of conduction.
[b] From Eq. (4).

Thus, taking into account the Heckelsberg criterion, as the electrical conductivity is lower under air than under nitrogen within all the temperature range considered, the CeO_2 and 1.1P/CeO_2 samples have a *n*-type semiconductor character (Fig. 1). For the 2.2P/CeO_2 sample the electrical conductivity under air was practically equal to that under nitrogen in the temperature range chosen. This suggests that this material could be an intrinsic semiconductor.

3.2.2. Variations of the electrical conductivity under air as a function of oxygen partial pressure

Fig. 2 shows the variations of σ as a function of oxygen pressure at 490 °C in a log–log plot. It clearly appeared that CeO_2 and 1.1P/CeO_2 samples were of the *n*-type under oxygen since $\partial\sigma/\partial P_{O_2} < 0$, while no dependence of σ on the oxygen pressure was observed for 2.2P/CeO_2 sample.

It is generally assumed that the electrical conductivity σ of *n*-type oxides varies as a function of partial pressure of oxygen P_{O_2} and temperature *T*, according to the equation:

$$\sigma(P_{O_2}, T) = C P_{O_2}^{-1/n} \exp\left(-\frac{\Delta H_c}{RT}\right) \quad (4)$$

where ΔH_c represents the enthalpy of conduction and *C* is a constant which only depends on various characteristics of the sample (charge and mobility of the charge carriers, number of contact points between grains, etc.) [1]. The value of the exponent *n* can be indicative of the nature of the defects in the solid, which generate charge carriers.

The values of the exponent *n* calculated for the different solids from the slopes of the log–log plots in Fig. 2, are presented in Table 2. From these values, only CeO_2 behaved according to a

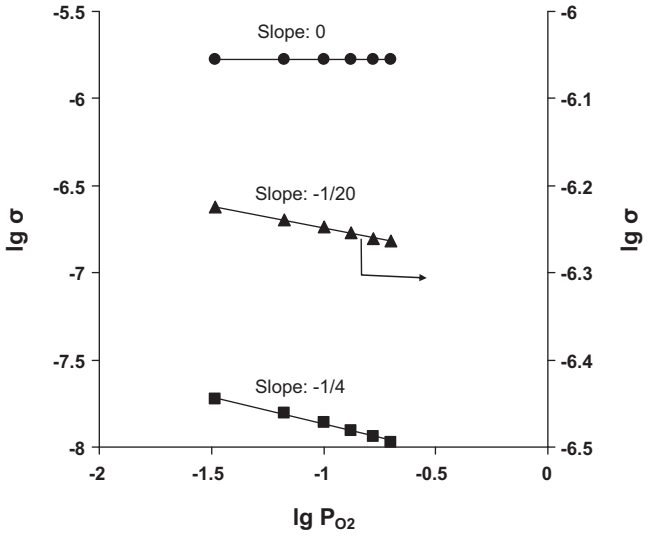

Fig. 2. Variation of σ as function of the oxygen pressure for CeO_2 (■), 1.1P/CeO_2 (▲) and 2.2P/CeO_2 (●) at 490 °C (P_{O2} in atm; σ in Ω^{-1} cm^{-1}).

simple conduction model with n approximately equal to 4. Such a value corresponds to the formation of singly ionized anionic vacancies according to the equations:

$$O_O^{\times} \rightleftarrows \tfrac{1}{2}O_{2(g)} + V_O^{\times} \quad (5)$$

$$V_O^{\times} \rightleftarrows V_O^{\bullet} + e' \quad (6)$$

where $O_O^{\times}$ represents an oxygen anion of the solid in regular lattice points, $V_O^{\times}$ a filled anionic vacancy, $V_O^{\bullet}$ a singly ionized anionic vacancy and e' a quasi-free electron.

The mass action law applied to Eqs. (5) and (6) gives:

$$K_5 = P_{O_2}^{1/2}[V_O^{\times}] \quad (7)$$

$$K_6 = \frac{[V_O^{\bullet}][e']}{[V_O^{\times}]} \quad (8)$$

The electroneutrality condition

$$[e'] = [V_O^{\bullet}] \quad (9)$$

combined with the mass action law yields:

$$\sigma \propto [e'] = (K_5K_6)^{1/2}P_{O_2}^{-1/4} \quad (10)$$

In the case of CeO_2 sample the log–log plot of σ as a function of P_{O_2} in air gives a descending straight line whose slope is indeed equal to $-1/4$ (Fig. 2). In addition, constants K_5 and K_6 follow the van't Hoff's law as a function of temperature:

$$K_5 = (K_5)_0 \exp\left(\frac{-\Delta H_5}{RT}\right) \quad (11)$$

$$K_6 = (K_6)_0 \exp\left(\frac{-\Delta H_6}{RT}\right) \quad (12)$$

where ΔH_5 and ΔH_6 are the enthalpies of reactions (5) and (6). Combining Eqs. (10), (11) and (12), one gets:

$$\sigma \propto [e'] = [(K_5)_0(K_6)_0]^{1/2} \exp\left[-\frac{\Delta H_5 + \Delta H_6}{2RT}\right] P_{O_2}^{-1/4} \quad (13)$$

Generally, the ionization energy of the first electron ΔH_6 can be neglected with respect to the formation enthalpy of anionic vacancies ΔH_5. Consequently, for CeO_2 the heat of formation of anionic vacancies is equal to $2E_c$, that is 279.6 kJ mol^{-1} (per mole of vacancies). This enthalpy is lower than that already reported for pure ceria (396 kJ mol^{-1}) [15] or other n-type oxide such as pure titania (342.7 kJ mol^{-1}) [19], but higher than that of tin oxide (226.0 kJ mol^{-1}) [20] and gives information about the lability of surface lattice oxygen anions able to react with isobutane. Under our experimental conditions, CeO_2 was active, as a n-type semiconductor, for the reaction of isobutane but gave high quantities of carbon oxides (Table 1) suggesting a high reactivity of the surface lattice oxygen anions in line with the relatively low enthalpy of formation of anionic vacancies observed.

The case study of the two phosphated ceria samples was more complex. Thus, for the 1.1P/CeO_2 sample the value of n was equal to 20 being significantly higher than 4 or 6 that respectively correspond to the formation of singly and doubly ionized vacancies. Such a phenomenon could be explained by a more complex model involving two different sources of electrons, one of them being independent of the partial pressure of oxygen:

$$\sigma = \sigma_1 + \sigma_2 \quad (14)$$

with $\sigma_1 = A(K_5K_6)^{1/2}P_{O_2}^{-1/4}$ and σ_2 independent of the partial pressure of oxygen P_{O_2}. Such a model has already been proposed for TiO_2 and related compounds [21] and vanadium antimonate based catalysts [10]. In the present case, a linear relationship was obtained when plotting the total conductivity σ as a function of $P_{O_2}^{-1/4}$ (Fig. 3). This confirmed the existence of a source of conduction electrons

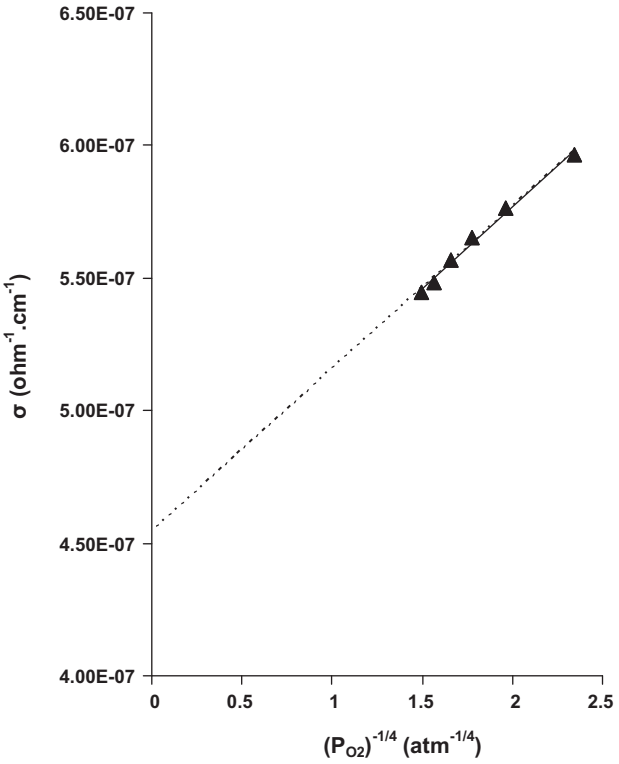

Fig. 3. Total conductivity σ versus $P_{O_2}^{-1/4}$ for 1.1P/CeO_2 at 490 °C.

whose nature was independent of oxygen pressure. Moreover, the y-intercept representing the conductivity σ_2 at the temperature concerned, it is possible to separate the two contributions. Thus, σ_2 being equal to $4.54 \times 10^{-7}\ \Omega^{-1}\ cm^{-1}$, σ_1 was calculated by subtracting σ_2 from σ according to Eq. (14) and was represented as a function of the oxygen pressure in a log–log plot (Fig. 4). The obtained plot exhibits the expected $-1/4$ slope, in line with the model proposed.

In the case of 2.2P/CeO_2 sample, the variation of σ with P_{O_2}, displayed in Fig. 2, shows that the electrical conductivity is practically independent of the oxygen pressure. This could lead to the conclusion that this material is rather an intrinsic semiconductor ($\partial\sigma/\partial P_{O_2} = 0$) as also suggested by the Heckelsberg criterion (Fig. 1). If that were the case, the theory would imply that the band-gap energy E_G should be equal to twice the activation energy of conduction E_c ($E_G = 2E_c$). Consequently, E_G should be equal to 119.2 kJ mol^{-1}, that is 1.24 eV. However, the band-gap energy determined from the UV spectrum of 2.2P/CeO_2 sample presented in Fig. 5 was equal to 3.2 eV. This value is quite different from that calculated, and the solid cannot be considered an intrinsic semiconductor under our conditions but an extrinsic one with sources of electrical charge carriers independent of oxygen pressure.

The observed increase of the electric conductivity of the samples caused by adding phosphorus to ceria and by increasing its content must be related to the P–CeO_2 interaction and could be explained taking into consideration a partial dissolution of P(V) in the lattice of ceria occurring via the substitution of P(V) to Ce(IV) ions in the surface and subsurface lattice positions of ceria. It is noteworthy that it has already been shown that P(V) ions can enter the fluorite CeO_2 structure by the substitution of Ce(IV) with P(V) [22]. This causes a doping effect according to the valence induction law of Verwey [23]. Each dissolved P(V) species shares four electrons with four O^{2-} neighbor anions, whereas the fifth electron is delocalized around the P(V) impurity as represented in Scheme 1. The P(V) impurities are associated with donor levels between the conduction band and

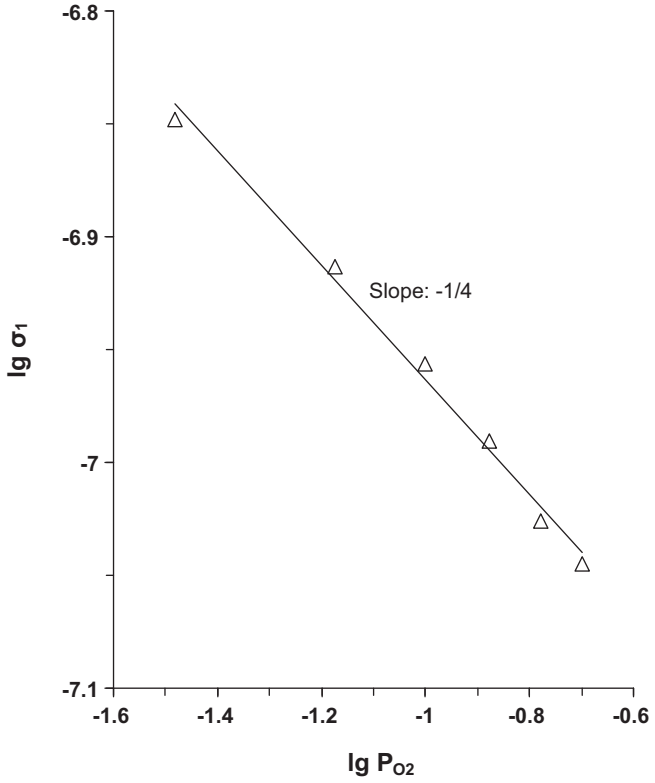

Fig. 4. Variation of σ_1 as function of the oxygen pressure for 1.1P/CeO_2 at 490 °C.

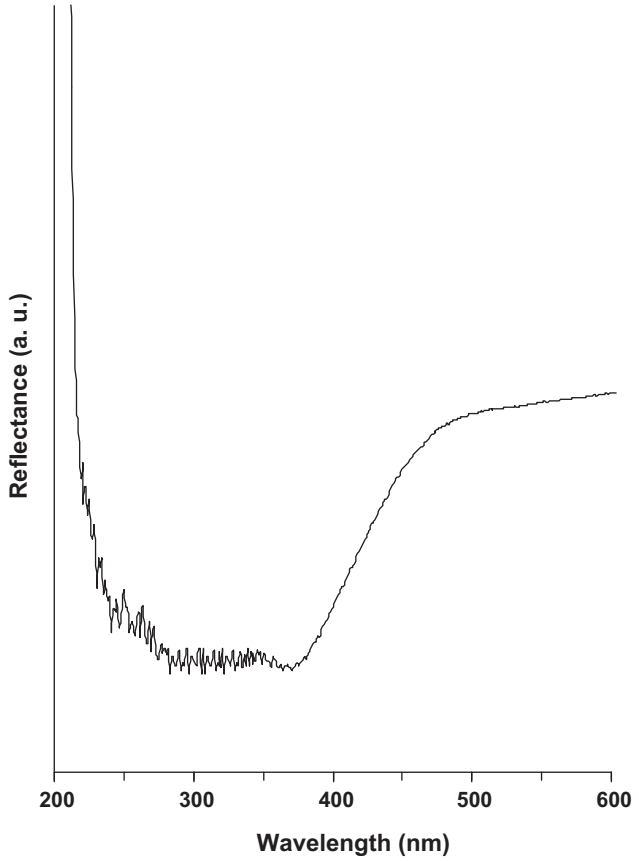

Fig. 5. UV–Vis spectrum of 2.2P/CeO_2 catalyst.

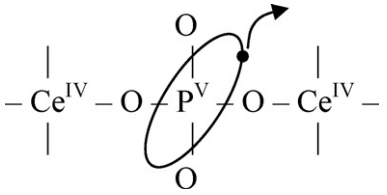

Scheme 1. Doping of ceria by P(V) dissolved species.

the valence band of ceria. A small energy is sufficient to ionize this donor level and to enable the fifth electron to reach the conduction band. This explains the observed decrease of the activation energy of conduction E_c (Table 2) under air caused by adding phosphorus to ceria and by increasing its content. Moreover, these substitution defects can be associated to the source of conduction electrons whose nature is independent of oxygen pressure evidenced in the phosphated ceria samples. On the other hand, the introduction of a higher valence cation, such as P(V), not only increases the substitution defects responsible for the increase of the charge carriers concentration but also reduces the vacancy population according to the reactions (15) and, to a lesser extent, (16):

$$P_2O_5 + V_O^{\bullet} \rightleftarrows 2P_{Ce}^{\bullet} + 5O_O^{\times} + e' \quad (15)$$

$$P_2O_5 + V_O^{\bullet\bullet} \rightleftarrows 2P_{Ce}^{\bullet} + 5O_O^{\times} \quad (16)$$

In that way we can explain the weakened dependence of the electrical conductivity on the oxygen pressure for 1.1P/CeO_2 and 2.2P/CeO_2 samples. Moreover, the consumption of oxygen vacancies results in lower surface lattice oxygen mobility and reactivity, in line with the hydrogen temperature-programmed reduction (H_2-TPR) data described in Ref. [17] and resumed in Table 3, explaining the observed decrease of the catalytic activity of the studied catalysts in the order CeO_2 > 1.1P/CeO_2 > 2.2P/CeO_2 for the reaction at 490 °C. The observed increase of the isobutene selectivity following the order CeO_2 < 1.1P/CeO_2 < 2.2P/CeO_2, can also be correlated with the decrease of the lattice oxygen mobility and lability suggested by the weakened dependence of the electrical conductivity on the oxygen pressure observed by adding phosphorus to ceria and by increasing its content.

It is noteworthy that the substitution of P(V) to Ce(IV) in the surface and subsurface lattice positions of ceria phase in the phosphated samples has already been suggested by the existence of low reducible Ce(IV) species in interaction with surface phosphorus, evidenced by hydrogen temperature-programmed reduction experiments [17].

3.2.3. *In situ* electrical conductivity measurements under catalytic conditions

To get information on the solids under conditions as close as possible to those of catalysis, the electrical conductivity measurements

Table 3
Peak maximum temperatures and H_2 consumptions in TPR experiments.[a]

Catalyst	Peak maximum temperature (°C)		Total H_2 consumption (μmol g^{-1})
	H_2 consumption (μmol g^{-1}) [%]		
CeO_2	530 216.5 [100]		216.5
1.1P/CeO_2	544 160.1 [78.6]	642 43.7 [21.4]	203.8
2.2P/CeO_2	617 45.1 [29.1]	678 109.6 [70.9]	154.7

[a] Data from Ref. [17].

were performed at a temperature within the reaction temperature range during sequential periods under air, under nitrogen, under isobutane–air mixture (reaction mixture with an air-to-isobutane molar ratio equal to 2.5) and under isobutane–nitrogen mixture (nitrogen-to-isobutane molar ratio equal to 2.5). The results obtained at 490 °C are displayed in Fig. 6.

The solids were heated from room temperature to 490 °C, at a heating rate of 5 °C/min in air flow at atmospheric pressure. After reaching the steady state under the air flow, nitrogen was introduced over the samples. As expected, the electrical conductivity increased for CeO_2 and 1.1P/CeO_2 samples and remained constant for 2.2P/CeO_2, confirming again the *n*-type character of CeO_2 and 1.1P/CeO_2 samples according to the Heckelsberg criterion. Then, air was again introduced over the samples and, after reaching the steady state, an isobutane–air mixture (reaction mixture) was passed over the samples. In the case of CeO_2, the electrical conductivity immediately increased abruptly by 4 orders of magnitude. The same increase of the electrical conductivity was observed for 1.1P/CeO_2, but within less than 2 orders of magnitude so that it becomes lower than that of CeO_2. These behaviors correspond to the *n*-type semiconductive character, since, for oxide semiconductors, the *n*-type criterion is $\partial\sigma/\partial P_{O_2} < 0$ or, considering isobutane as a reductant, $\partial\sigma/\partial P_{i\text{-}C_4H_{10}} > 0$. Surprisingly, for 2.2P/CeO_2 sample the electrical conductivity slightly decreased under the isobutane–air flow. This behavior corresponds rather to the *p*-type character, since, for oxide semiconductors, the *p*-type criterion is $\partial\sigma/\partial P_{O_2} > 0$ or, considering isobutane as a reductant, $\partial\sigma/\partial P_{i\text{-}C_4H_{10}} < 0$.

After reaching the steady state under the isobutane–air flow, air was again introduced over the samples. The electrical conductivity decreased immediately and reached a plateau for CeO_2 and 1.1P/CeO_2 samples confirming the *n*-type character of both solids. In the case of 2.2P/CeO_2 sample the electrical conductivity slightly increased, but the plateau corresponding to the new steady state under air was not the same as before the isobutane–air mixture sequence, suggesting a new state of the solid that obviously corresponds to a reduced oxide.

After reaching the steady state under the air flow, the isobutane–nitrogen mixture was introduced in contact with the samples and then, after reaching the steady state under this mixture, the air sequence was repeated for observing the reversibility of the phenomena. Again, an important increase of the electric conductivity was observed for CeO_2 and 1.1P/CeO_2 samples corresponding to their *n*-type semiconductive character. Under air their electrical conductivities decreased immediately and reached a plateau confirming the reversibility of the phenomena observed. For the 2.2P/CeO_2 sample, the electrical conductivity slightly decreased under the isobutane–nitrogen flow suggesting again a *p*-type character for this sample. Under air, the electrical conductivity of the 2.2P/CeO_2 sample increased and reached a plateau identical to that reached after the isobutane–air sequence, but different from that corresponding to the initial state suggesting an irreversible reduction of the solid.

The reversible redox process observed in the case of the CeO_2 and 1.1P/CeO_2 samples during successive sequences under isobutane–air mixture or isobutane–nitrogen mixture and air can be explained as follows. Isobutane is oxidized by reaction with surface lattice oxygen anions, thus partially reducing the surface. The increase of σ can be ascribed to the creation of anionic vacancies, $V_O^{\times}$, by reduction of the solid by isobutane:

$$O_O^{\times} + i\text{-}C_4H_{10} \rightarrow i\text{-}C_4H_8 + H_2O + V_O^{\times} \quad (17)$$

followed by the spontaneous ionization of the anionic vacancies according to the following equations:

$$V_O^{\times} \rightleftarrows V_O^{\bullet} + e' \quad (18)$$

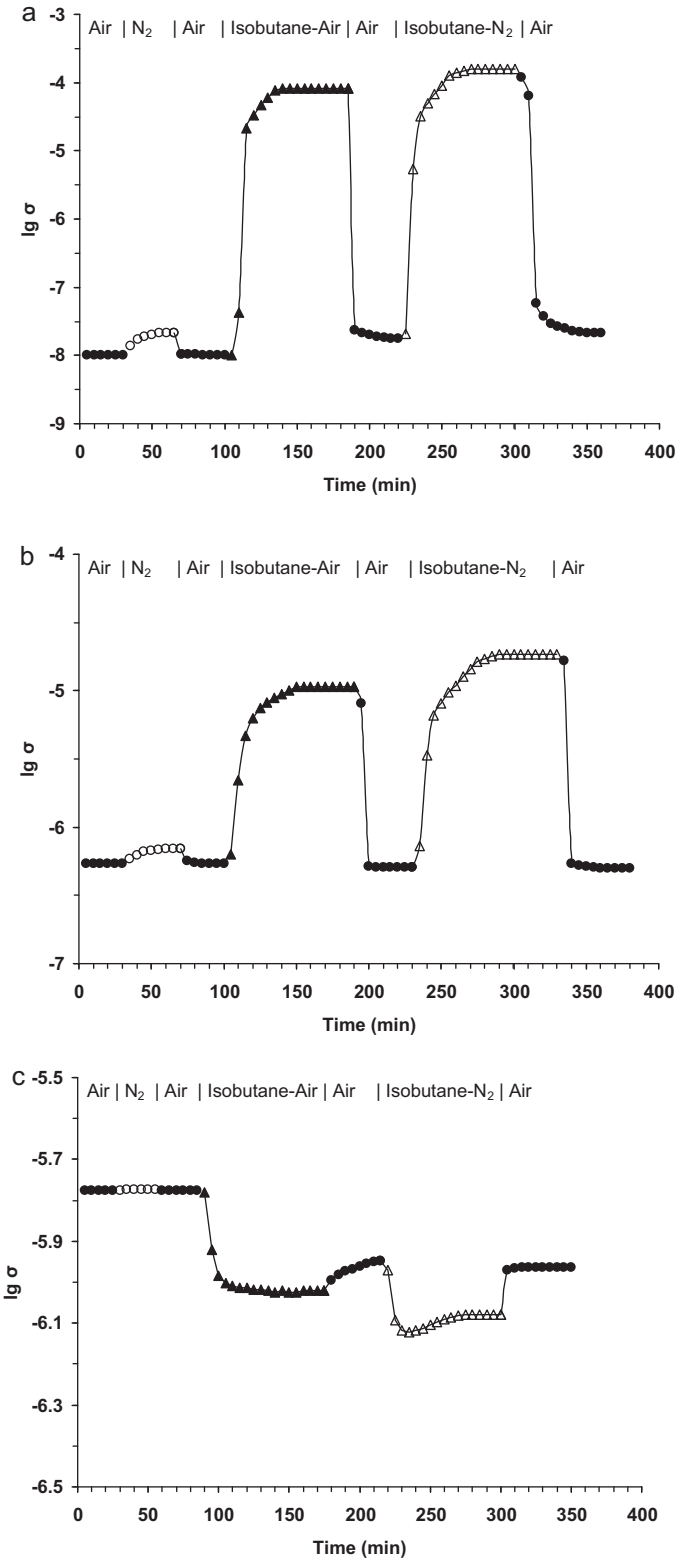

Fig. 6. Variation of the electrical conductivity under sequential exposures to air (●), nitrogen (○), isobutane–air mixture (reaction mixture) (▲) and isobutane–nitrogen mixture (△) for CeO_2 (a), 1.1P/CeO_2 (b) and 2.2P/CeO_2 (c) at 490 °C (σ in Ω^{-1} cm^{-1}).

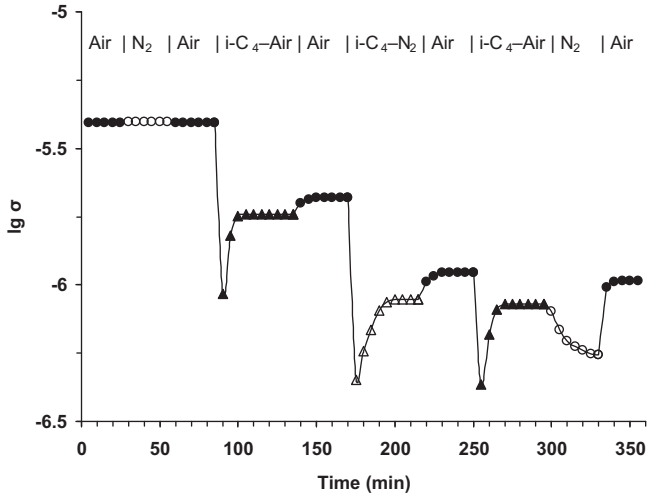

Fig. 7. Variation of the electrical conductivity under sequential exposures to air (●), nitrogen (○), isobutane–air mixture (reaction mixture) (▲) and isobutane–nitrogen mixture (△) for 2.2P/CeO_2 at 610 °C (σ in Ω^{-1} cm^{-1}).

$$V_O^{\bullet} \rightleftarrows V_O^{\bullet\bullet} + e' \quad (19)$$

where $O_O^{\times}$ represents an oxygen anion of the solid in regular lattice points (O^{2-}), $V_O^{\times}$ a filled anionic vacancy, $V_O^{\bullet}$ a singly ionized anionic vacancy and $V_O^{\bullet\bullet}$ a doubly ionized anionic vacancy.

The release of free electrons into the conduction band of the solid accounts for the observed increase in electrical conductivity. The subsequent introduction of air over the samples restores the initial value of σ indicating the refilling of the previously created anionic vacancies by dissociation of oxygen and capture of free electrons according to the reactions:

$$\frac{1}{2}O_2 + V_O^{\bullet} + e' \rightleftarrows O_O^{\times} \quad (20)$$

$$\frac{1}{2}O_2 + V_O^{\bullet\bullet} + 2e' \rightleftarrows O_O^{\times} \quad (21)$$

This behavior is in agreement with a Mars–van Krevelen type mechanism [24]. Note that, in our case, the reactions (19) and (21) involving doubly ionized anionic vacancies are negligible as suggested by the variation of the electrical conductivity as a function of oxygen partial pressure.

The case of 2.2P/CeO_2 sample is more complex. It seems to behave as a *p*-type semiconductor with positive holes, $h^{\bullet}$, as the main charge carriers under the reaction conditions. For confirming this behavior and for explaining the inverse order of activity observed at temperatures higher than 570 °C, that is 2.2P/CeO_2 > 1.1P/CeO_2 > CeO_2, electrical conductivity measurements were performed with 2.2P/CeO_2 at 610 °C during sequential periods under air, under nitrogen, under isobutane–air mixture and under isobutane–nitrogen mixture, the results obtained being presented in Fig. 7. It can be observed that, as expected, the electrical conductivity of the solid remained almost constant during air–nitrogen–air sequential periods. When the air flow was replaced by the isobutane–air mixture (reaction mixture), the electrical conductivity firstly decreased abruptly and then increased to reach the plateau corresponding to the steady state. This corresponds to the combination of two opposite phenomena, an initial reduction by isobutane followed by a kind of reoxidation of the surface region as already observed for vanadium pyrophosphate under *n*-butane [4] and confirms the *p*-type behavior of the 2.2P/CeO_2 catalyst under the isobutane–air mixture. After reaching the steady state under the isobutane–air flow, a new sequence of air was introduced over the 2.2P/CeO_2 sample. The electrical conductivity slightly increased to reach a plateau which is different from that observed under air before the isobutane–air mixture sequence suggesting a new state of the solid that obviously corresponds to a reduced oxide. After reaching the new steady state under the air flow, a sequence of isobutane–nitrogen mixture was introduced over the sample. The electrical conductivity firstly decreased abruptly and then increased slowly to reach the plateau corresponding to the steady state. This confirms the *p*-type character of the 2.2P/CeO_2 catalyst in the presence of isobutane. When air was again introduced over the sample, the electrical conductivity increased immediately and reached a plateau corresponding to a new σ value different from the previous value under air suggesting that the solid was further and irreversibly reduced by the isobutane–nitrogen mixture. The air was replaced by a new isobutane–air flow when the solid was again reduced, then a sequence of nitrogen was admitted over the sample. One can observe that the electrical conductivity decreased to reach the plateau corresponding to the new steady state under nitrogen. When air was finally introduced over the sample, the electrical conductivity increased and reached a plateau that did not correspond to the fully oxidized initial solid but was similar to the value observed during the last sequence under air suggesting a redox behavior of the 2.2P/CeO_2 catalyst. It is noteworthy that for the reduced solid, the electrical conductivity under nitrogen was lower than that under air. This confirms that, according to Heckelsberg criterion, it behaves as a *p*-type semiconductor.

The results obtained with 2.2P/CeO_2 catalyst showed that it behaves as an extrinsic semiconductor with sources of electrical charge carriers independent of oxygen pressure under air but became a *p*-type semiconductor under the reaction mixture (isobutane–air). Such a phenomenon can only be explained by a change in the structure of the solid, at least in the surface region [10]. The existence of such an irreversible change was supported by the fact that after the first reduction, the solid underwent redox cycles that were not completely reversible and remained characteristic of a *p*-type semiconductor. For explaining this behavior we have to consider the 2.2P/CeO_2 catalyst as a mixture of two conducting phases, CeO_2 and $CePO_4$, as evidenced by XRD. It is well known that in a mixture of two conducting oxides, the overall conductivity of the sample becomes governed by the more conducting component above a certain percentage, called the percolation threshold [13]. In our case, the $CePO_4$ is rather a surface phase as expected taking into consideration the method of preparation used for the phosphated samples and as confirmed by the XPS analysis [17]. For confirming that the surface $CePO_4$ phase was responsible for the electrical conductivity behavior of the 2.2P/CeO_2 sample under sequences of reactants, electrical conductivity measurements of $CePO_4$ (Alfa Aesar) were performed at 610 °C during sequential periods under air, isobutane–air mixture, nitrogen and isobutane–nitrogen mixture. The results obtained are displayed in Fig. 8. It can be observed that, when the air flow was replaced by the isobutane–air mixture, the electrical conductivity decreased abruptly and reached a plateau corresponding to the steady state. This confirms the *p*-type behavior of the $CePO_4$ sample similar to 2.2P/CeO_2. When air was introduced over the $CePO_4$ sample, the electrical conductivity increased immediately and reached a plateau corresponding to a σ value strongly different from the initial value suggesting that the reoxidation of the reduced solid was not totally reversible. This phenomenon was similar to that already observed for 2.2P/CeO_2 catalyst. After reaching the new steady state under air flow, a sequence of isobutane–nitrogen mixture was introduced over the $CePO_4$ sample. Again, the electrical conductivity decreased abruptly and reached a plateau corresponding to the steady state of the reduced solid. This confirms the *p*-type character of $CePO_4$ in the presence of isobutane. Then, after a nitrogen sequence, air was again introduced over the sample and the electrical conductivity increased immediately and reached a plateau that

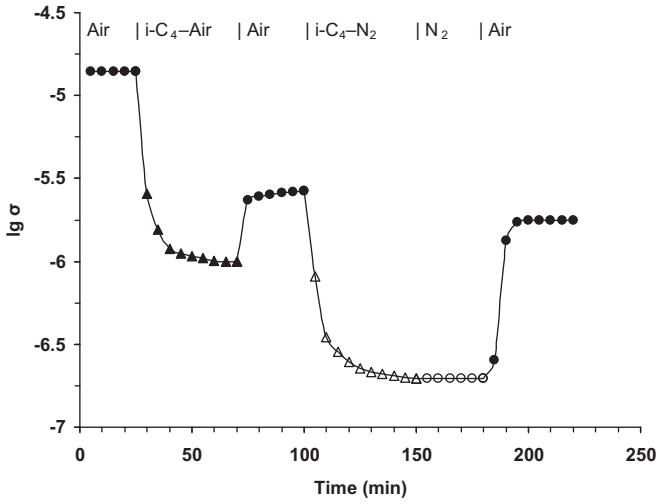

Fig. 8. Variation of the electrical conductivity under sequential exposures to air (●), isobutane–air mixture (reaction mixture) (▲), isobutane–nitrogen mixture (△) and nitrogen (○) for $CePO_4$ at 610 °C (σ in Ω^{-1} cm^{-1}).

did not correspond to a fully oxidized initial solid. This behavior is very similar to that of the 2.2P/CeO_2 catalyst confirming that its electrical conductivity behavior is mainly determined by the cerium (III) phosphate phase evidenced on its surface. Moreover, the activation energy of conduction E_c under air at atmospheric pressure, determined for $CePO_4$ sample from the semi-log plot [$\log\sigma = f(1/T)$] in the temperature range from 400 to 660 °C (Fig. 9), was equal to 0.65 eV. This value is strongly similar to that obtained for the 2.2P/CeO_2 sample, i.e. 0.62 eV, suggesting that the charge carrier formation needs similar energies in the two samples [25]. Consequently, the *p*-type conductivity observed for the 2.2P/CeO_2 catalyst after reduction during the sequence under isobutane–air mixture flow could be explained considering only the contribution of the surface cerium (III) phosphate phase to the overall electrical conductivity of the 2.2P/CeO_2 sample and regarding this phase as a Ce(IV)-doped $CePO_4$. Note that, it has already been shown that a ceria-doped $CePO_4$ catalyst was active and selective in isobutane

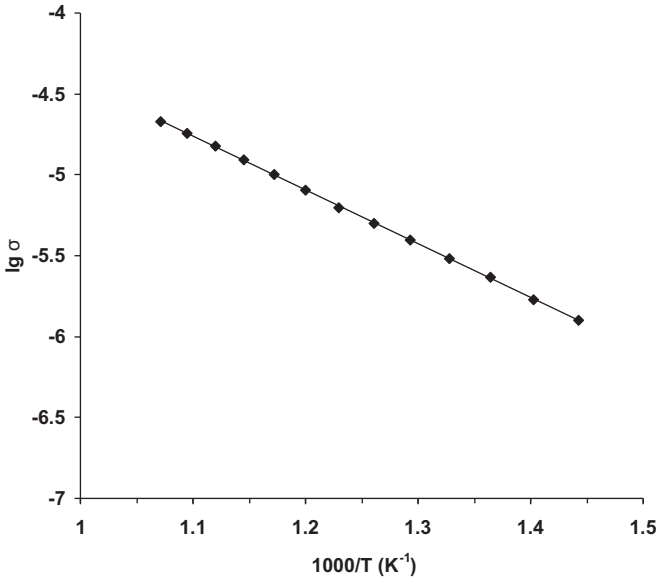

Fig. 9. Arrhenius plot for the electrical conductivity σ of $CePO_4$ under air (σ in Ω^{-1} cm^{-1}).

oxydehydrogenation reaction [26]. In this case, the following electrochemical equilibrium can be assumed:

$$Ce^{4+} \rightleftarrows Ce^{3+} + h^{\bullet} \quad (22)$$

If one considers that from the chemical point of view, a positive hole corresponds to an electron vacancy in the valence band of lattice $O_O^{\times}$ anions, i.e. the "chemical site" of a positive hole corresponds in fact to a lattice $O_O^{\bullet}$ anion [4], according to the reaction:

$$O_O^{\times} + h^{\bullet} \rightleftarrows O_O^{\bullet} \quad (23)$$

the transformation of isobutane into isobutene over 2.2P/CeO_2 catalyst can be written:

$$i\text{-}C_4H_{10} + O_O^{\bullet} \rightarrow i\text{-}C_4H_9^{\bullet} + (HO^-)^{\bullet} \quad (24)$$

$$i\text{-}C_4H_9^{\bullet} + O_O^{\bullet} \rightarrow i\text{-}C_4H_8 + (HO^-)^{\bullet} \quad (25)$$

Water elimination generates oxygen vacancies, according to the reaction:

$$2(HO^-)^{\bullet} \rightleftarrows H_2O_{(g)} + O_O^{\times} + V_O^{\bullet\bullet} \quad (26)$$

These vacancies must be filled in by gaseous oxygen in order to reoxidize the solid:

$$\frac{1}{2}O_{2(g)} + V_O^{\bullet\bullet} \rightarrow O_O^{\times} + 2h^{\bullet} \quad (27)$$

This suggests that the overall reaction mechanism on 2.2P/CeO_2 catalyst can also be assimilated to a Mars–van Krevelen type mechanism [24], but in this case the oxydehydrogenation reaction involves surface lattice O^- species ($O_O^{\bullet}$), whereas for CeO_2 surface lattice O^{2-} anions ($O_O^{\times}$) are involved. The O^- species are known to be quite active species for alkanes' oxidation [4], explaining the highest activity observed for 2.2P/CeO_2 catalyst at 610 °C. The weak variations of the electrical conductivity observed in that case suggest a low concentration of O^- species on the surface in line with the high isobutene selectivity measured during the catalytic process. If the O^- species were too numerous on the surface, they might promote isobutane combustion rather than oxydehydrogenation.

The equilibrium (22) responsible for the generation of the positive holes obviously involves the low reducible Ce(IV) species interacting with the phosphate phase evidenced by H_2-TPR data described in Ref. [17] and resumed in Table 3. Taking it into consideration, one could explain the lowest activity of the 2.2P/CeO_2 catalyst in the series studied at low temperature as well as its highest activity at high temperatures where the low reducible Ce(IV) species are more easily reduced.

1.1P/CeO_2 catalyst has an intermediate behavior between CeO_2 and 2.2P/CeO_2: it can also be considered as a mixture of two phases, CeO_2 and $CePO_4$, as evidenced by DRX, but the overall electrical conductivity is governed by the ceria phase. On the other hand, this solid contains a small, but nevertheless significant concentration of low reducible Ce(IV) species interacting with the phosphate phase as evidenced in H_2-TPR experiments (Table 3). Consequently, it is reasonable to consider that, in this case, the reaction mechanism involves mainly surface lattice O^{2-} anions but a mechanism involving surface lattice O^- species especially at high temperatures cannot be excluded.

All these results explain well the catalytic behavior of the ceria and phosphated ceria catalysts as well as the compensation effect in catalysis observed.

4. Conclusion

Pure ceria as well as two surface-phosphated ceria, 1.1P/CeO_2 and 2.2P/CeO_2, catalysts for isobutane oxydehydrogenation, were characterized by in situ electrical conductivity measurements. It

has been established that all the catalysts were *n*-type semiconductors under air. Their electrical conductivity increased while their activation energy of conduction decreased following the order CeO_2 < 1.1P/CeO_2 < 2.2P/CeO_2 suggesting the formation of substitution defects of Ce(IV) with P(V) in the phosphated ceria samples. Under isobutane–nitrogen mixture or under isobutane–air mixture, CeO_2 and 1.1P/CeO_2 remained *n*-type semiconductors whereas 2.2P/CeO_2 became *p*-type semiconductor, its electrical conductivity behavior being governed by the $CePO_4$ phase.

For the 2.2P/CeO_2 catalyst the oxydehydrogenation reaction involves surface lattice O^- species, whereas for CeO_2 surface lattice O^{2-} anions are involved. For the 1.1P/CeO_2 catalyst the reaction mechanism involves mainly surface lattice O^{2-} anions but a mechanism involving surface lattice O^- species, especially at high temperatures, must be considered. These results explained the difference in catalytic performances encountered on the three solids as well as the compensation effect in catalysis evidenced. In all cases the overall reaction mechanism can be assimilated to a Mars and van Krevelen mechanism.

References

[1] J.-M. Herrmann, in: B. Imelik, J.C. Védrine (Eds.), Catalyst Characterization, Physical Techniques for Solid Materials, Plenum Press, New York, 1994, chapter 20.
[2] H. Ponceblanc, J.M.M. Millet, G. Coudurier, J.-M. Herrmann, J.C. Védrine, J. Catal. 142 (1993) 373–380.
[3] J.-M. Herrmann, J. Disdier, F.G. Freire, M.F. Portela, J. Chem. Soc. Faraday Trans. 91 (1995) 2343–2348.
[4] J.-M. Herrmann, P. Vernoux, K.E. Béré, M. Abon, J. Catal. 167 (1997) 106–117.
[5] I.-C. Marcu, J.M.M. Millet, J.-M. Herrmann, Catal. Lett. 78 (2002) 273–279.
[6] I.-C. Marcu, I. Săndulescu, Y. Schuurman, J.M.M. Millet, Appl. Catal. A 334 (2008) 207–216.
[7] L.M. Madeira, J.-M. Herrmann, F.G. Freire, M.F. Portela, F.J. Maldonado, Appl. Catal. A 158 (1997) 243–256.
[8] L.M. Madeira, J.-M. Herrmann, J. Disdier, M.F. Portela, F.G. Freire, Appl. Catal. A 235 (2002) 1–10.
[9] J.-M. Herrmann, F. Villain, L.G. Appel, Appl. Catal. A 240 (2003) 177–182.
[10] J.M.M. Millet, I.-C. Marcu, J.-M. Herrmann, J. Mol. Catal. A 226 (2005) 111–117.
[11] G. Mitran, A. Urdă, I. Săndulescu, I.-C. Marcu, React. Kinet. Mech. Catal. 99 (2010) 135–142.
[12] I. Popescu, I. Săndulescu, Á. Rédey, I.-C. Marcu, Catal. Lett. 141 (2011) 445–451.
[13] J.-M. Herrmann, J. Disdier, Catal. Today 56 (2000) 389–401.
[14] A. Trovarelli (Ed.), Catalysis by Ceria and Related Materials, Imperial College Press, London, 2005.
[15] M. Mogensen, N.M. Sammes, G.A. Tompsett, Solid State Ionics 129 (2000) 63–94.
[16] C. Bozo, N. Guilhaume, J.-M. Herrmann, J. Catal. 203 (2001) 393–406.
[17] I.-C. Marcu, M.N. Urlan, Á. Rédey, I. Săndulescu, C. R. Chim. 13 (2010) 365–371.
[18] L.F. Heckelsberg, A. Clark, G.C. Bailey, J. Phys. Chem. 60 (1956) 559–561.
[19] J.-M. Herrmann, J. Catal. 118 (1989) 43–52.
[20] J.-M. Herrmann, J.L. Portefaix, M. Forissier, F. Figueras, P. Pichat, J. Chem. Soc. Faraday Trans. 75 (1979) 1346–1355.
[21] J.M. Herrmann, J. Disdier, Catal. Today 20 (1994) 135–152.
[22] M. Boaro, A. Trovarelli, J.H. Hwang, T.O. Mason, Solid State Ionics 147 (2002) 85–95.
[23] E.J.W. Verwey, P.W. Haijman, F.C. Romeijn, G.W. Van Oosterhout, Philips Res. Rep. 5 (1950) 173–187.
[24] S. Mars, N. van Krevelen, Chem. Eng. Sci 9 (1954) 41–57 (Special Supplement).
[25] V. Raghavan, Materials Science and Engineering: A First Course, 5th ed., Prentice-Hall of India Private Limited, New Delhi, 2004, p. 368.
[26] Y. Takita, X. Qing, A. Takami, H. Nishiguchi, K. Nagaoka, Appl. Catal. A 296 (2005) 63–69.